Integrated Control of DER Placement and Network Reconfiguration in EV-Charging Distribution Systems Using Multi-Optimization Techniques

Paramet Nuamkoksung[1], Wutthichai Sa-nga-ngam[1], Kittiwong Suthamno[1], Thongchai Klayklueng[1], Supapradit Marsong[2,3], Somchat Sonasang[4], Krischonme Bhumkittipich[5,], Dieu Ngoc Vo[6,7], Krittidet Buayai[1], Kaan Kerdchuen[1] and Yuttana Kongjeen[1,*]

[1] Intelligent Power System and Energy Research (IPER), Department of Electrical engineering, Faculty of Engineering and Technology, Rajamangala University of Technology Isan, Nakhon Ratchasima, Thailand [2] Elevating Studio (Thailand) Ltd., Bangkok, Thailand

[3] Department of Electrical Engineering, Thonburi university, Bangkok, Thailand

[4] Department of Electrical Elements and Wireless Devices Research Unit (EEWDRU), Faculty of Industrial Technology, Nakhon Phanom University, Nakhon Phanom, Thailand

[5] Department of Electrical Engineering, Faculty of Engineering, Rajamangala University of Technology Thanyaburi (RMUTT), Pathum Thani 12110, Thailand

[6] Department of Power Systems, Ho Chi Minh City University of Technology (HCMUT), Ho Chi Minh City, Vietnam [7] Vietnam National University Ho Chi Minh City, Ho Chi Minh City, Vietnam

*Corresponding Email : yuttana.ko@rmuti.ac.th

Received February 1, 2025, Revised March 11, 2025, Accepted March 13, 2025, Published June 30, 2025

Abstract. *The integration of distributed energy resources (DERs), such as photovoltaic (PV) systems, into power distribution networks is critical for enhancing grid reliability, reducing power losses, and promoting renewable energy adoption. Fast charging stations (FCSs), due to their high energy demand, further complicate grid operation, particularly in maintaining voltage stability and coordinating power supply. While previous studies often address DERs placement or control strategies in isolation, this study proposes a unified framework that optimizes both the placement and sizing of DERs in combination with advanced grid control mechanisms. The proposed approach uses a hybrid of three metaheuristic algorithms: Grey Wolf Optimization (GWO), Particle Swarm Optimization (PSO), and Whale Optimization Algorithm (WOA). The multi-objective formulation focuses on minimizing power loss and cost, improving voltage profiles, and reducing the L-index. A notable contribution of this work is the integration of Volt/Var and power factor (PF) management into the optimization process, which enables practical grid stabilization under steady-state conditions. The methodology is applied to the IEEE 33-bus distribution network and validated through simulation. Results indicate that the hybrid method performs better than traditional single-algorithm approaches, achieving significant power loss reductions and voltage improvements. These findings provide a practical roadmap for distribution system planning under high DERs and FCS penetration.*

Keywords:

Distributed Energy Resources, Electric Vehicle Charging Station, Grey Wolf Optimization, Particle swarm optimization, Whale optimization, L-index, Voltage Stability, Power Loss Reduction

1. Introduction

The transformation of power distribution systems through the integration of electric vehicles (EVs) and distributed generation (DG) sources has introduced significant challenges in network management, optimization, and infrastructure planning. This evolution necessitates advanced strategies for network reconfiguration, distributed energy resource (DER) coordination, and charging infrastructure integration to ensure efficient, reliable, and sustainable operation. Modern distribution networks must satisfy multiple objectives, including power loss reduction, voltage profile enhancement, and optimal EV charging station (EVCS) placement, while maintaining overall system stability.

Network reconfiguration (NR) and DG allocation have emerged as key strategies to address these objectives. Recent advances in meta-heuristic optimization methods have shown strong potential in enhancing distribution network performance. Samman et al. [1] developed a two-stage Firefly Algorithm (FA) that simplifies complex networks using simplified network graphs (SNG),

significantly improving computational efficiency. Salau et al. [2] extended this work by proposing a modified Selective Particle Swarm Optimization (SPSO) algorithm, effectively minimizing voltage deviation and power losses. Other developments include a sine-cosine algorithm with Lévy flights for simultaneous NR and DG allocation [3], and the Antlion Optimizer (ALO), which incorporates power quality indices into optimization objectives [4]. To manage the increasing complexity of modern distribution systems, researchers have proposed various multi-objective frameworks. Fast heuristic methods for harmonic minimization [5] have demonstrated effectiveness in improving power quality with low computational overhead. Cloud theory-based approaches [6] have been applied to model uncertainty in feeder reconfiguration, particularly in systems integrating renewable energy sources. Integrated strategies for DG and capacitor placement have also been introduced to optimize reactive power support [7]. Fu et al. [8] proposed phase demand balancing models to improve dispatch capabilities in active distribution networks. Planning for EVCS deployment introduces additional complexity in distribution network operation. Wang et al. [9] presented a unified framework for crew dispatch and restoration planning, highlighting the importance of coordinated infrastructure development. Pal et al. [10] examined EVCS expansion planning based on user behavior and charging demand patterns. Yenchamchalit et al. [11] addressed the joint optimization of photovoltaic (PV) systems and EVCS placement, while Mazumder et al. [12] introduced reactive power compensation techniques for EV charging infrastructure. These studies emphasize the importance of integrated planning approaches that consider both grid performance and user-centric factors. Advanced strategies for EVCS planning continue to evolve. Lima et al. [13] incorporated locational transmission tariffs into NR strategies, while Fukui et al. [14] developed placement models that account for randomly distributed rooftop PV. Zeb et al. [15] investigated optimal siting of multiple types of charging stations in both commercial and residential settings. Gan et al. [16] and Chitgreeyan et al. [17] explored elastic demand models for fast-charging station (FCS) deployment, introducing capacity planning strategies aligned with temporal demand variations. More recently, hybrid and enhanced meta-heuristic algorithms have been applied to address complex optimization problems in distribution networks. An improved equilibrium optimization algorithm was proposed in [18] for simultaneous NR and DG allocation. Enhanced versions of the Marine Predator Algorithm have shown improved performance across varying load scenarios. Shaheen et al. [19] introduced a chaotic search group algorithm for joint optimization of network configuration and DER integration.

However, many existing studies focus on isolated components of distribution system optimization typically addressing either DER placement or EVCS planning without considering their combined impacts on network reconfiguration and voltage regulation. Moreover, few frameworks integrate steady-state operational control strategies such as Volt/Var and power factor (PF) regulation, which are essential for maintaining voltage stability under high DER penetration. Challenges related to scalability and practical implementation in large-scale distribution networks also remain underexplored. This study addresses these research gaps through the following key contributions:

1. A hybrid meta-heuristic framework integrating GWO, PSO, and WOA is developed for simultaneous FCS placement, DER allocation, and network reconfiguration to minimize power losses and improve voltage profiles.

2. To improve voltage stability and reactive power management under steady-state operating conditions, we incorporate Volt/Var control and power factor regulation

3. The proposed approach is validated on the IEEE 33-bus test system across various loading scenarios, demonstrating scalability and operational effectiveness.

4. Environmental impacts, including DER penetration and CO_2 emissions, are evaluated under optimized and conventional control strategies.

2. Problem Formulation and Mathematical Models

The mathematical model system used for solving optimal power flow under the fast-charging stations (FCSs) and distributed energy resources (DERs) interface that is related by the power flow equation, photovoltaic power plant, fast charging station, evaluation indices and optimization techniques can be presented as follows:

A. Power Flow Equations

This research is integrating the power flow equations of propose that combining with power balance of the grid and apparatus are follows [20]:

$$P_i^{grid} + P_i^{PV} - P_i^{FCS} - P_i^{load} = \sum_{j=1}^{N} |V_i||V_j| \left(G_{ij}\, cos\, \theta_{ij} + B_{ij}\, sin\, \theta_{ij}\right) \quad (1)$$

$$Q_i^{\text{grid}} + Q_i^{\text{PV}} - Q_i^{\text{FCS}} - Q_i^{\text{load}} = \sum_{j=1}^{N} |V_i||V_j| \left(G_{ij}\, sin\, \theta_{ij} - B_{ij}\, cos\, \theta_{ij}\right) \quad (2)$$

Where: $P_i^{\text{grid}}, Q_i^{\text{grid}}$: Active and reactive power from the grid at bus$i$,P_i^{PV}, Q_i^{PV}: Active and reactive power generated by DG at bus$i$,Active and reactive power consumed by FCS at bus$i$, $P_i^{\text{load}}, Q_i^{\text{load}}$: Active and reactive power consumed by loads at bus i

B. Photovoltaic (PV) Power Generation

The DERs are represented by the PV power plant. The active power output of a solar PV system is

determined by solar irradiance, temperature and system efficiency:

$$P_{PV}(t) = G(t) \cdot A_{PV} \cdot \eta_{PV} \quad (3)$$

Where: $P_{\mathrm{PV}}(t)$: PV system's active power output (in MW) at time t, $G(t)$: Solar irradiance (in kW /m^2) at time$t$, A_{PV}: Total area of PV panels (in m^2), η_{PV} : Overall efficiency of the PV system, including panel, inverter, and system losses. The module efficiency η_{module} is temperature-dependent:

$$\eta_{module} = \eta_{module,STC}[1 \cdot \beta \cdot (T_c - T_{STC})] \quad (4)$$

Where: η_{module} : Module efficiency at Standard Test Conditions (STC), β:Temperature coefficient of power (%/°C),T_C:Cell temperature (°C),T_{STC}: Standard Test Condition temperature (25°C).

The cell temperature T_C can be approximated as:

$$T_c = T_a + \left(\frac{G(t)}{G_{ref}}\right) \cdot NOCT \quad (5)$$

Where: $\mathrm{T_a}$: Ambient temperature (^{0}C)., $\mathrm{G_{ref}}$: Reference irradiance (typically 1000 W/m^2)., NOCT : Nominal operating cell temperature (°C).

Reactive Power Control of PV power plant is used to control the power and voltage of the point of common coupling (PCC). The PV can be controlled by Volt/Var and PF control that related by the reactive power output can be defined as:

$$Q_{PV} = \sqrt{S_{PV}^2 - P_{PV}^2} \quad (6)$$

1. Reactive Power (Q) Calculation (PF Control):

$$Q = P \cdot tan(cos^{-1}(PF)) \quad (7)$$

2. Volt/Var Control Linear interpolation based on voltage:

$$Q_{mvar} = Q_{max} + \frac{(V_{pu} - V_{low}) \cdot (Q_{min} - Q_{max})}{(V_{high} - V_{low})} \quad (8)$$

Where: Q_{PV}: Reactive power generated by the PV system (in MVar), S_{PV}^2: Apparent power capacity of the PV system (in MVA), P_{PV}: Active power generated by the PV system (in MW).

C. Electric Vehicle Charging Station (EVCS)

Main of these devices are related by power electronic conversion from AC to DC or called by rectifier circuits and connected thought by wire conductor to the battery system on the electric vehicles. The EVCS can be categorized by many types of charging system and application of the charging rate as fast charging, flash charging, slow charging etc. So, many researchers are studying the characteristics of EVCS for using to find and analyze the impact of electric vehicles to the grid. This research used the constant power model of the EVCS as follows [21]:

$$P_i^{FCS} = P_i^{fixed}, \quad Q_i^{FCS} \approx 0.05 \cdot P_i^{FCS} \quad (9)$$

D. Technical Performance Indices

These indices assess the technical benefits of the proposed optimization and control strategies.

1) Total power loss reduction is used to evaluate the reduction in total active power losses (Ploss) in the system:

$$P_{\mathrm{loss}} = \sum_{i=1}^{N} P_{(\mathrm{line,i})} = \sum_{i=1}^{N} \left(I_{\mathrm{line,i}}^2 \cdot R_{\mathrm{line,i}}\right) \quad (10)$$

Where $P_{\mathrm{line},i}$ is the active power loss in line i.

2) Voltage profile improvement is used to analyze the voltage magnitude (Vi) across all buses. The voltage deviation index (VDI) is selected to analyze this problem and can be expressed as:

$$\mathrm{VDI} = \sum_{i=1}^{N} |V_i - V_{\mathrm{nom}}| \quad (11)$$

Where: V_{nom} is the nominal voltage (e.g., 1.0 p.u.) [21].

3) Line Loading is used to evaluate the loading percentage of each line to ensure no thermal violations.

$$Loading\ percentage = \frac{S_{line}}{S_{(line,max)}} \cdot 100 \quad (12)$$

Where: $S_{(\mathrm{line,max})}$ is the line's thermal capacity.

4) Voltage Stability Index (L- Index) is delivered by computing the L-index for each line to assess voltage stability [22]:

$$L - index_i = 1 - \left|\frac{Y_{ij} \cdot V_j}{|V_i|^2}\right| \quad (13)$$

Where:Z_{ij} :Impedance a the line between buses i and j, Q_i: Reactive power at bus i,$|V_i|^2$:Voltage magnitude at bus i.

E. Environmental Performance Indices

Environmental performance indices (EPIs) are related to the power generation reduced from using green energy. This research focuses on PV power generation that can be generated in a solar time on average of 4.5 hr. per day. The EPIs are represented as follows [23]:

1) CO_2 emission reduction Estimate the reduction in emissions due to PV integration with 4.5 hr. per day.

$$CO_2^{\mathrm{saved}} = P_{\mathrm{PV}} \cdot T \cdot E_{factor} \cdot 8760\ \mathrm{hr/y} \quad (14)$$

Where: : CO_2^{saved}Reduction in CO_2 emissions (in kg). T is operational time (in 4.5 hours per day). $E_{factor}$is Grid emission factor (in kg CO_2/MWh).

2) Renewable energy penetration is used to measure the quantify the percentage of renewable energy in total power generation as follows:

$$\%Renewable = \frac{P_{PV}}{P_{total}} \cdot 100 \quad (15)$$

F. The Multi-Optimization Techniques (MOTs)

The MOTs are used to solve the optimal control of the propose. Many methodologies of optimization techniques are developed in the word of research, this research is focused on popularly used to solve the problem of the electrical power system as follows:

1) Gray Wolf Optimization (GWO)

The GWO algorithm is a metaheuristic optimization technique inspired by the leadership hierarchy and hunting behavior of gray wolves in nature. It can be an important equation as follows [24,29]:

1.1 Key Concepts of GWO:
Gray Wolf Hierarchy:

- Alpha (α): The leader of the pack, responsible for decision-making and guiding the hunt. Represents the best solution in the optimization process.
- Beta (β): The second-in-command, assisting the alpha. Represents the second-best solution.
- Delta (δ): The subordinate wolves helping α and β. Represents the third-best solution.
- Omega (ω): The lowest-ranked wolves, following the higher-ranked wolves. These represent the rest of the solutions

1.2 Hunting behavior:
The algorithm mimics the gray wolves' hunting process, which consists of encircling the prey, attacking the prey, searching for prey, respectively.

1.3 Mathematical model
1.3.1 Encircling prey as follows:

$$\vec{D} = \left|\vec{C} \cdot \overrightarrow{X_p}(t) - \overrightarrow{X_p}(t)\right| \quad (16)$$

$$\overrightarrow{X_p}(t+1) = \overrightarrow{X_p}(t) - \overrightarrow{A} \cdot \vec{D} \quad (17)$$

Where: $\vec{X}(t)$ is current position of the wolf. $\overrightarrow{X_p}(t)$ is position of the prey (or best solution). $\vec{A}$ is a coefficient vector to control exploration/exploitation. $\vec{C}$ is random coefficient vector.

1.3.2 Updating the positions of the wolves based on the α, β, and δ wolves:

$$\overrightarrow{X_p}(t+1) = \frac{\overrightarrow{X_1}+\overrightarrow{X_2}+\overrightarrow{X_3}}{3} \quad (18)$$

Where $\overrightarrow{X_1}$, $\overrightarrow{X_2}$ and $\overrightarrow{X_3}$are computed based on α, β and δ.

1.3.3 Control Parameters are related by using parameter as follows:

$\vec{A}=2\vec{a}\,\overrightarrow{r_1}-\vec{a}$ is balances exploration exploitation (gradually decreases a a from 2 to 0).
$\vec{C}=2\vec{r}_2$ is enhances randomness.
$\overrightarrow{r_1}$ and $\overrightarrow{r_2}$ is random vectors in the range [0, 1].

2) Particle Swarm Optimization (PSO)

The PSO is an optimization method inspired by the movement behavior of animal swarms, such as flocks of birds or schools of fish. The main idea of PSO is to use a group of particles to explore the search space to find the best solution, where each particle represents a possible solution to the problem.

The main equations of Particle Swarm Optimization (PSO) are as follows [25]:

Velocity Update:

$$v_i(t+1) = w \cdot v_i(t) + c_1 \cdot r_1 \cdot (pbest_i - x_i(t)) + c_2 \cdot r_2 \cdot (gbest - x_i(t)) \quad (19)$$

Position Update:

$$x_i(t+1) = x_i(t) + v_i(t+1) \quad (20)$$

Where:
$v_i(t)$ is the velocity of particle i at time t. $x_i(t)$ is the position of particle$i$at time t.w is inertia weightc_1, c_2 is cognitive and social learning coefficients**.** r_1, r_2 are random values between 0 and 1**.** $pbest_i$:The best position of particle**.**$gbest$ The global best position (best position of the entire swarm)**.**

3) Whale Optimization Algorithm (WOA)

WOA is a metaheuristic optimization technique inspired by the bubble-net hunting strategy of humpback whales.

3.1 The modelling of WOA

This behavior is modeled through two key mechanisms are Exploitation: represented by encircling and spiraling toward prey and Exploration: achieved by searching for new prey in the search space.

3.2 Mathematical Modeling of WOA [26]:

- Encircling Prey:

Whales estimate the position of the prey (optimal solution) and adjust their position toward it:

$$\vec{D}=|\vec{C}\cdot\vec{X}^*(t)-\vec{X}(t)| \quad (21)$$

$$\vec{X}(t+1)=\vec{X}^*(t)-\vec{A}\cdot\vec{D}| \quad (22)$$

Where: $\vec{X}^*(t)$ is best-known solution (position of prey). $\vec{X}(t)$ is the current position of the whale. $\vec{A}\cdot\vec{D}$ |coefficients controlling exploration and exploitation.

- Spiral Updating Position:

Whales swim around the prey in a spiral path:

$$\vec{X}(t+1)=\vec{D}'\cdot e^{bl}\cdot\cos(2\pi l)+\vec{X}^*(t) \quad (23)$$

Where: $b$is Shape constant of the spiral. l is Random number in search space. $\vec{D}'$ is the distance between whale and prey.

- Search for Prey:

Whales randomly explore the search space by moving away from the best-known solution:

$$\vec{X}(t+1) = \vec{X}_{rand} - \vec{A} \cdot \vec{D} \quad (24)$$

Where $\vec{X}_{rand}$ is a randomly chosen solution.

3. Methodology

This section is to present the research step for preparing the simulation case. Static state power flow is applied to solve and explore the purpose based on pandapower [27] as follows:

A. Hybrid - Objective Function

A hybrid-objective function is formulated to minimize power losses, L-index and VDI. Penalty factors are included to address voltage violations, reverse power flow, line overloading, constraints.

The optimization aims to minimize a hybrid-objective function F combining several goals:

$$F = \omega_1 \cdot P_{\text{loss}} + \omega_2 \cdot max(L-index) + \omega_3 \cdot VDI + P_{\text{penalty}} \quad (25)$$

Where: P_{loss} is total power losses in the network.$L-index$ is maximum voltage stability index. VDI is voltage deviation index from nominal values. P_{penalty}: Penalty for constraint violations.,$\omega_1, \omega_2, \omega_3$: Weights assigned to each objective are set up 0.333.

B. Constraint and Limits

1. Voltage magnitude at each bus must remain within permissible limits:

$$V \ |V_i| Buses_{max_{min}} \quad (26)$$

2. Line Thermal Limits
The loading on each line must not exceed its thermal capacity:

$$S_{ij} = \sqrt{P_{ij}^2 + Q_{ij}^2} \leq S_{ij}^{max}, \quad \forall (i,j) \in Lines \quad (27)$$

3. The FCS grid connection:
The grid supplies active and reactive power to balance the system:

$$P_i^{\text{FCS}}, \quad Q_i^{\text{grid}} \geq 0 \quad (28)$$

4. Power Balance of Bus
The PV contributes to the overall power balance at its bus:

$$P_{\text{bus}} = P_{\text{load}} - P_{PV} + P_{FCS} \quad (29)$$

5. Power Factor (PF) Constraints
The PF of DG must remain within its operational limits:

$$PF_{\text{min}} \leq PF_N \leq PF_{\text{max}}, \quad \forall N; \text{number of DG} \quad (30)$$

6. Renewable Power Output Constraints
Power generated by PV systems must respect resource availability:

$$0 \leq P_{\text{PV}} \leq P_{\text{PV}}^{\text{max}} \quad (31)$$

Penalty Terms
The penalty for constraint violations is expressed as:

$$P_{\text{penalty}} = P_v + P_r + P_l \quad (32)$$

Where: Pv: Penalty for voltage violations $|V| < 0.95\text{p.u. or} |V| > 1.05\text{p.u.}$,$P_r$: Penalty for reverse power flow.,P_l: Penalty for line loading exceeding 100%.

C. Primary Distribution Power Systems

The IEEE 33-bus system is selected to evaluate the impact of FCS integration on the power grid. It operates with a total load of 3.72 MW and 2.30 MVar, consisting of 32 radial transmission lines [28]. This study categorizes the system into six zones based on load type: industrial plants (1,020 kW) have the highest demand, followed by department Stores (740 kW) and tourist areas (625 kW). Other zones, including housing, Theme Parks, and miscellaneous loads, range between 420-460 kW. This classification supports efficient power distribution and resource management as shown in Table 1 and Figure 1. The FCSs are defined by using passive conceptual of the sizing and location by Table 4.

Table 1 The Load categories zone

Zone (No.)	Categories	Bus (No.)	Total Load (kW)
1	Housing estate	2, 19, 20, 21, 22	460
2	Industrials	3, 23, 24, 25	1,020
3	Theme Parks	4, 5, 6, 26, 27, 28	420
4	Tourist Area	7, 8, 9, 10, 11, 12	625
5	Department	29, 30, 31, 32, 33	740
6	Other	13, 14, 15, 16, 17,18	450

Table 2 Parameter of the multi-optimization techniques

Parameters	Description	Value/Range
Objective	Hybrid of the total power loss, VDI, max L-index with p.u. base.	-
Method	Optimal solution for line control, PVs placement	Multi-optimization techniques
FCS Cap.	Fast charging station capacity	50 kW
FCS Number	Fast charging station number	6 (Fix Position)
PV Cap.	PV power plant capacity	0.1 - 3.0 MW

Table 2 Parameter of the multi-optimization techniques (Cont.)

Parameters	Description	Value/Range
Tie-switch number	The number of Tie-switch	6 (Variables)/Loop
PF. Control	Power factor control limit	0.85 - 1.00
Volt/Var control	Volt/var control limit	-2 Mvar to 2 MVar
Voltage Limits	Acceptable voltage range	0.95–1.05 p.u.
Line loading limit	Acceptable line loading range	Thermal limit of line each section
Iteration	Solving the problem limit range	100
GWO:		
N	Number of Wolves	100
PSO:		
N	Number of particles	100
c_1	Coefficient of Local acceleration	2.5
c_2	Coefficient of global acceleration	2.5
w	Weight inertia	1
WOA:		
	Number of Whales	100

Table 2 shows the parameters of the multi-optimization techniques for using to find optimal conditions. So that, all basic parameters of each optimization needed to equip for comparing the performance.

Table 3. defines optimization variables across cases. Tie-switch control (X1-X5) starts from Case 3, while PVs Position & Sizing (X6-X11) are introduced in Case 4 onward. PF Control (X8-X14) is applied in Cases 4-6, while Volt/Var control (X10-X14) is used in Cases 7-9 for voltage regulation. Cases 6 and 9 implement the most comprehensive optimization strategy. However, the limitation of the tie switch controller is constrained by the number of operations allowed per day. Therefore, optimal control must be managed accordingly in real power systems.

Table 4. compares FCSs, Tie-Line Control, and PV placement strategies. Case 1 is the base scenario, while Cases 2-3 add FCSs and tie-line control. Cases 4-6 integrate 1-3 PV units with PF control, optimizing power flow. Cases 7-9 apply Volt/Var control for better voltage regulation. Cases 6 and 9 (Multi-PVs with 3 units) achieve the best power balance and voltage stability, confirming optimal tie-line and PV placement effectiveness.

4. Simulation and Results

The result of this research is divided into 3 main sections that are based by the multi-optimization techniques of the purpose. The case study from Table 1 is used to solve the problem and results in evaluating the power system improving under optimal conditions. The FCSs are installed by fixing location and sizing which is the electrical power system needed to manage the system for supporting the demand from the FCSs. However, this study focuses on the photovoltaic power generation

system and network reconfiguration control for managing the power generation and transmission line control. Network control is defined by using radial system, does not islanding mode and loop system. The comparison of each case can be presented by the table, network graph and voltage magnitude profiles and line loading. Power system analysis tool is applied by network graph and combined with heat map of voltage magnitude and line loading. The best case of each optimization technique is selected to present the graph for benchmarking the performance and analysis.

Table 5. highlights the effectiveness of GWO in optimizing PV placement and tie-switching. Baseline cases (1 & 2) exhibit high power losses (202.677 kW and 225.295 kW) with poor voltage deviation (1.700 p.u. and 1.830 p.u.). Tie-switching alone (Case 3) reduces power loss to 167.019 kW (25.81% improvement), while adding PVs (Case 4) further lowers losses to 84.687 kW, improving voltage deviation to 0.467 p.u.. The most optimized scenario, Case 5, with 1,353 kW and 1,403 kW

PVs at Buses 9, 31 and tie-switching at 9, 6, 13, 30, 23, achieves the lowest power loss (50.776 kW, 77.45% reduction) and the best voltage stability (0.224 p.u.) with optimal PF control (0.850, 0.850). Cases 6-9, despite larger PVs, do not surpass Case 5, underscoring the importance of strategic PV placement and switching. These results confirm GWO's effectiveness in enhancing distribution network performance.

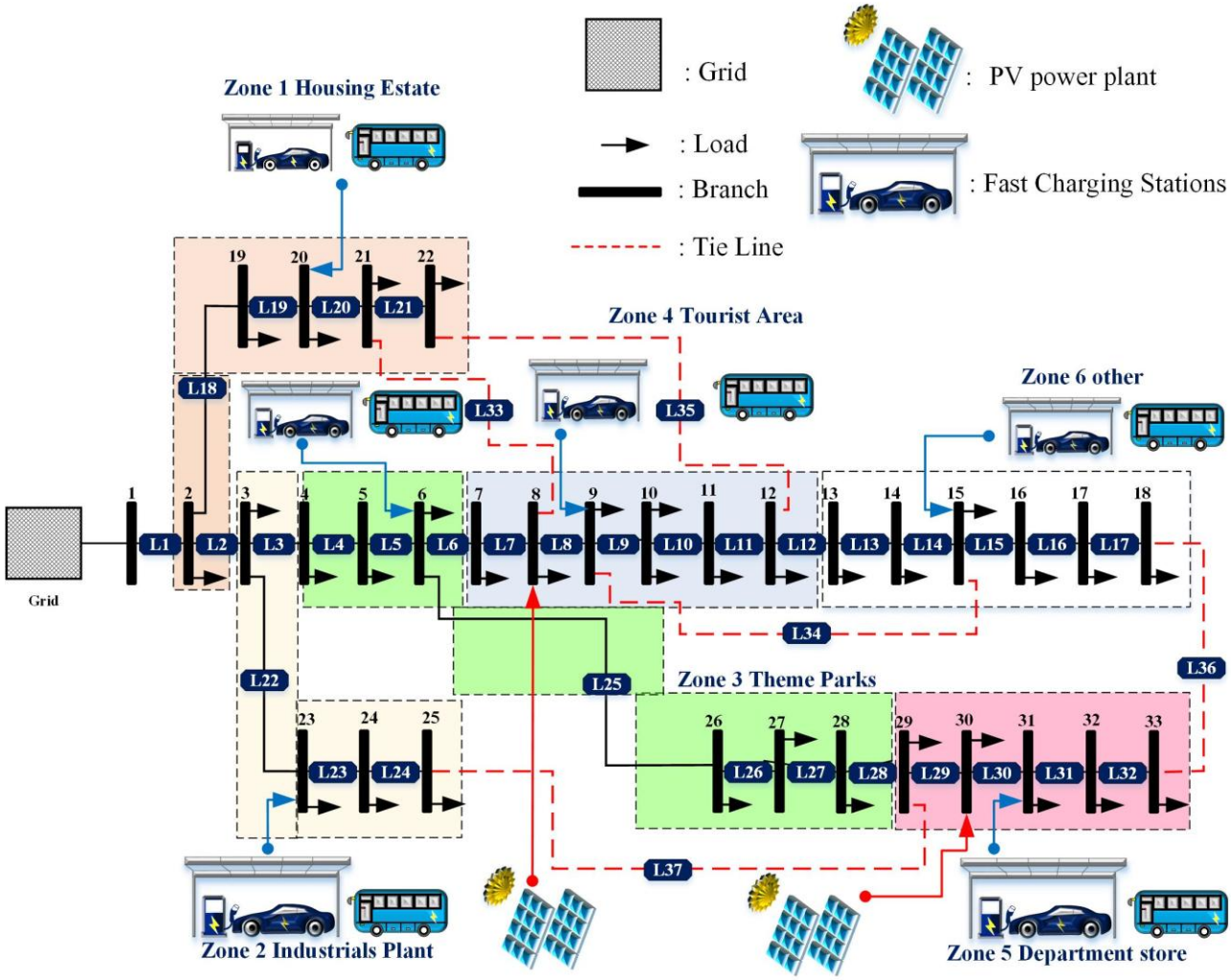

Fig.1 The IEEE 33 bus testing system for solving the optimal Tie -switch control, PVs placement of the propose

Table 3 Definition of variables for using optimal control from the propose.

Case	Variable No. X1 to X_n																
	Tie-Switch Control					PVs Position			PVs Sizing			PF. Control			Volt/Var Control		
1	-	-	-	-	-	-	-	-	-	-	-	-	-	-	-	-	-
2	-	-	-	-	-	-	-	-	-	-	-	-	-	-	-	-	-
3	X1	X2	X3	X4	X5	-	-	-	-	-	-	-	-	-	-	-	-
4	X1	X2	X3	X4	X5	X6	-	-	X7	-	-	X8	-	-	-	-	-
5	X1	X2	X3	X4	X5	X6	X7		X8	X9		X10	X11	-	-	-	-
6	X1	X2	X3	X4	X5	X6	X7	X8	X9	X10	X11	X12	X13	X14	-	-	-
7	X1	X2	X3	X4	X5	X6	-	-	X7	-	-	-	-	-	X8	-	-
8	X1	X2	X3	X4	X5	X6	X7		X8	X9	-	-	-	-	X10	X11	-
9	X1	X2	X3	X4	X5	X6	X7	X8	X9	X10	X11	-	-	-	X12	X13	X14

Table 4 The study case of the Optimal Line Control and Distributed Energy Resources Placement

Case Study	FCS Location	Tie Line/PVs	FCS			PVs				
			Sizing	Number of Station	Total Capacity of FCS	Location	Sizing	Number of PVs	Total Capacity of PVs	Control Type
	(Bus No.)	(Line No.)	(kW)	(Unit)	(kW)	(Bus No.)	(kW)	Unit	(kW)	(kW)
1	Base Case	Disable = 33,34,35,36,37	-	-	-	-	-	-	-	-
2	6,9,15,20,23,31	Disable = 33,34,35,36,37	50	6	300	-	-	-	-	-
3	6,9,15,20,23,31	Optimal Tie-Line Control	50	6	300	-	-	-	-	-
4	6,9,15,20,23,31	Optimal Tie-Line Control +PV	50	6	300	OPT	OPT	1	OPT	PF
5	6,9,15,20,23,31	Optimal Tie-Line Control and Multi-PVs (2 PVs)	50	6	300	OPT	OPT	2	OPT	PF
6	6,9,15,20,23,31	Optimal Tie-Line Control and Optimal Multi-PVs (3 PVs)	50	6	300	OPT	OPT	3	OPT	PF
7	6,9,15,20,23,31	Optimal Tie-Line Control + PV	50	6	300	OPT	OPT	1	OPT	Volt/Var
8	6,9,15,20,23,31	Optimal Tie-Line Control and Optimal Multi-PVs (2 PVs)	50	6	300	OPT	OPT	2	OPT	Volt/Var
9	6,9,15,20,23,31	Optimal Tie-Line Control and Optimal Multi-PVs (3 PVs)	50	6	300	OPT	OPT	3	OPT	Volt/Var

Table 5 Simulation Results of the GWO

Case	PVs		Tie Switch (No.)	Total power loss		Voltage Deviation		PF Control
				Before	After	Before	After	
	(kW)	(Bus No.)		(kW)	(kW)	(p.u.)	(p.u.)	
1	-	-	-	202.677	-	1.700	-	-
2	-	-	-	225.295	-	1.830	-	-
3	-	-	8, 5, 13, 16, 27	225.295	167.019	1.830	1.262	-
4	1,164	18	7, 6, 12, 29, 27	225.295	84.687	1.830	0.467	0.891
5	**1353, 1403**	**9, 31**	**9, 6, 13, 30, 23**	**225.295**	**50.776**	**1.830**	**0.224**	**0.850, 0.850**
6	1506, 715, 1212	30,10,25	10, 4, 12, 14, 27	225.295	52.566	1.830	0.328	0.999,0.856,0.884
7	2,909	29	10, 4, 13, 35, 22	225.295	208.895	1.830	1.597	0.997
8	100, 2777	8, 30	10, 3, 11, 15, 21	225.295	246.559	1.830	2.243	0.997, 0.856
9	1570, 1092, 1080	29, 21, 31	32, 18, 11, 28, 26	225.295	148.67	1.830	0.874	0.977, 0.856, 0.884

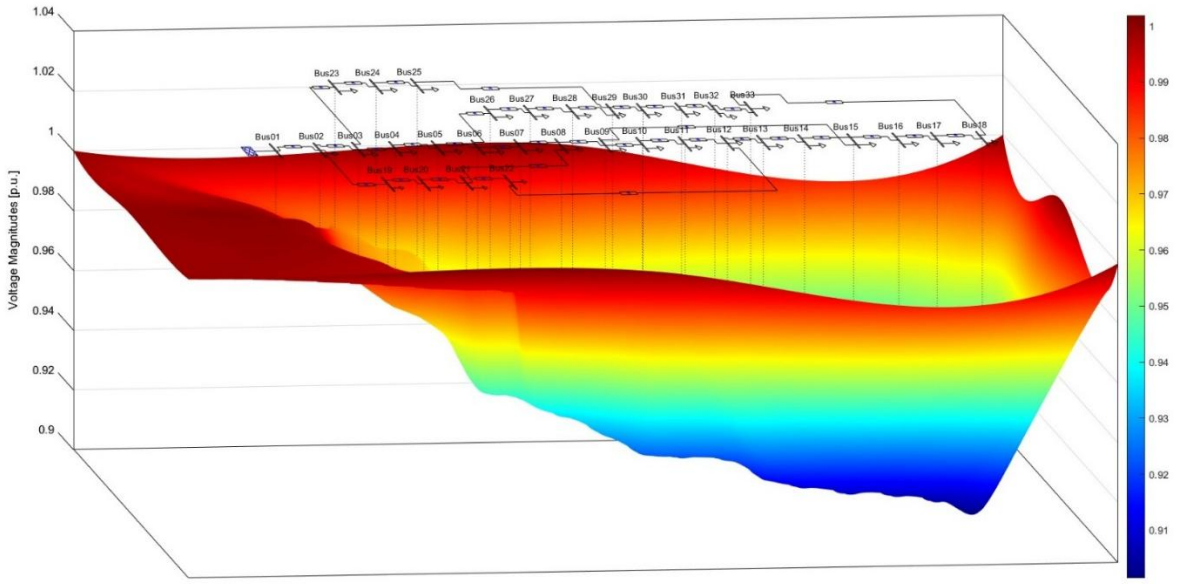

Fig. 2 The bus voltage magnitudes of Case 2

Figure. 2 visualizes bus voltage magnitudes in the IEEE 33-bus system for Case 2, showing voltage distribution under FCS integration. Higher voltages (~1.0 p.u.) appear near the substation, while lower voltages (0.91 p.u.) occur in distant buses, indicating weak voltage regulation. The voltage drop worsens with increased distance, highlighting the impact of FCS on system stability and the need for tie-switching or PV integration to improve voltage profiles. In deep details, the color red represents higher voltages, and blue indicates lower voltages which is minimum voltage: 0.907 p.u. maximum voltage: 0.100 p.u. average voltage: 0.945 p.u.

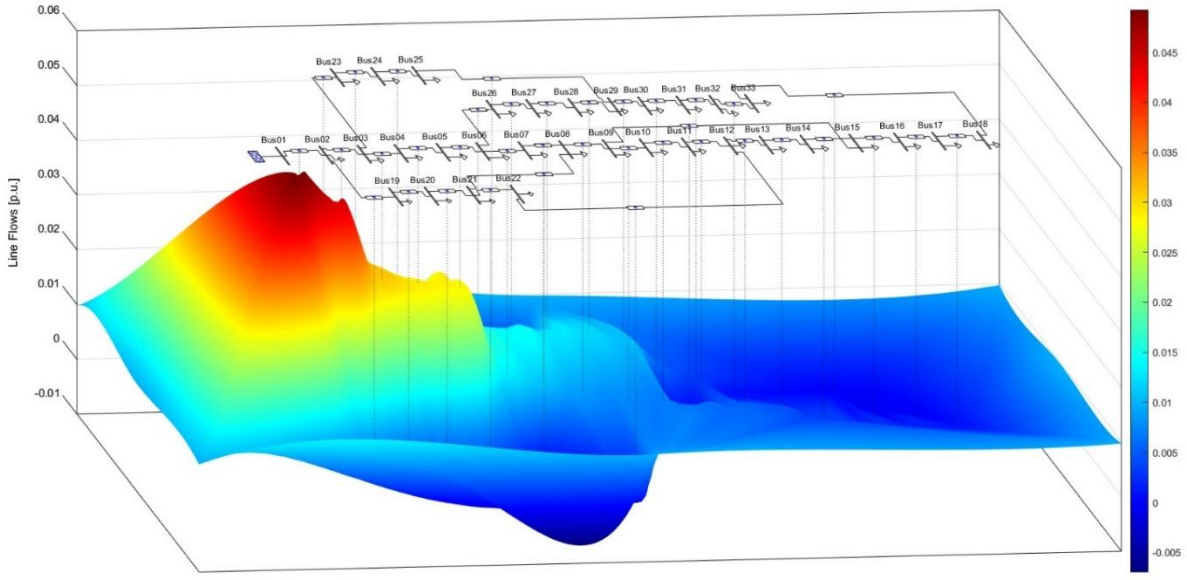

Fig. 3 The transmission lines power flow of Case 2

Figure. 3 visualizes power flow in the IEEE 33-bus system under FCS integration and network control. Red zones near the source indicate high power flows, while blue regions show weaker distribution in distant buses. The sharp variations highlight network congestion, confirming the need for tie-switching and PV integration to enhance stability and reduce losses.

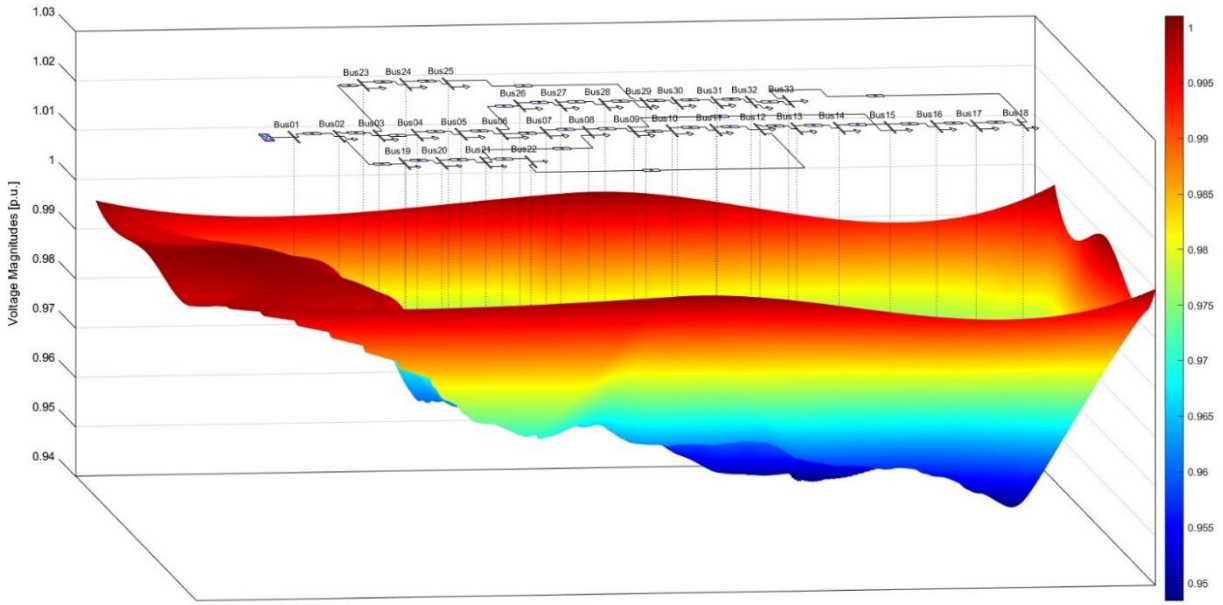

Fig. 4 The bus voltage magnitudes of Case 3

Figure.4 shows the bus voltage magnitudes for Case 3 with tie-switch control. Compared to Case 2, voltage stability improves, with fewer low-voltage areas. Higher voltages (0.99-1.0 p.u.) dominate, while voltage drops (0.95 p.u.) are minimized. This confirms that tie-switching enhances voltage regulation and system stability. The voltage profile with a colour gradient, where red represents higher voltages and blue indicates lower voltages which is minimum voltage: 0.931 p.u. maximum voltage: 1.000 p.u. average voltage: 0.963 p.u.

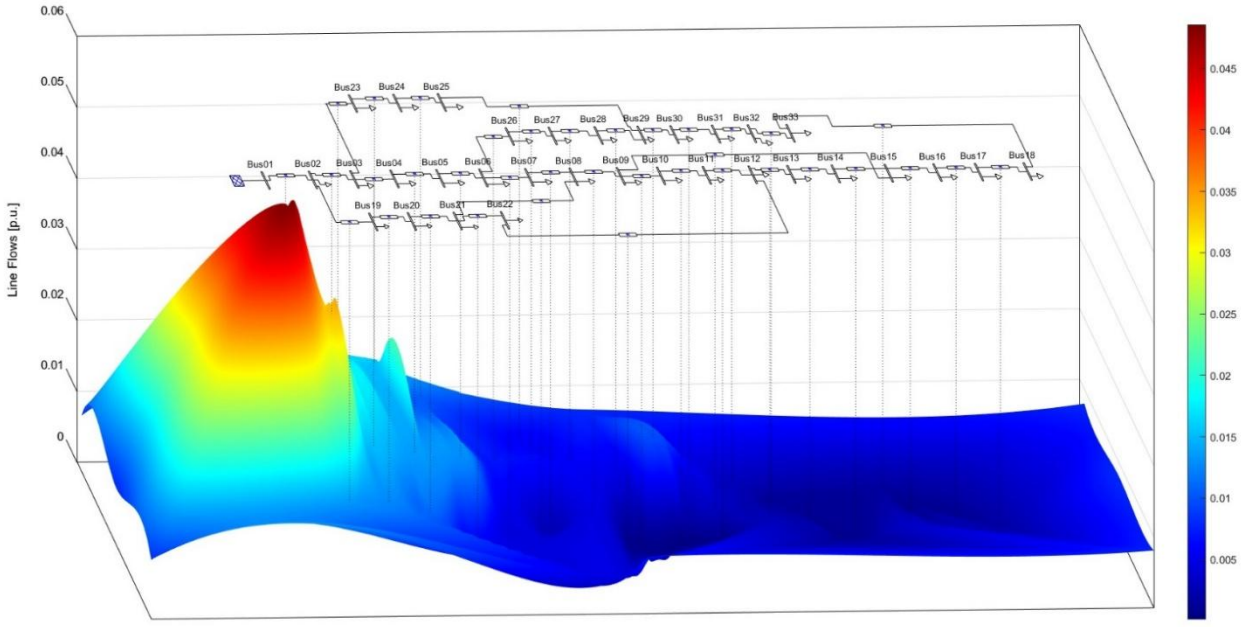

Fig. 5 The transmission lines power flow of Case 3

Figure. 5 shows power flow in the IEEE 33-bus system with tie-switch control. Compared to Case 2, congestion is reduced, flow is more balanced, and losses are minimized. Smaller red zones indicate improved network stability and efficiency. These results demonstrate that effectively manages power flow, reducing losses and enhancing network performance.in: min: 0.000 p.u., max: 0.022 p.u., Avg: 0.003 p.u.

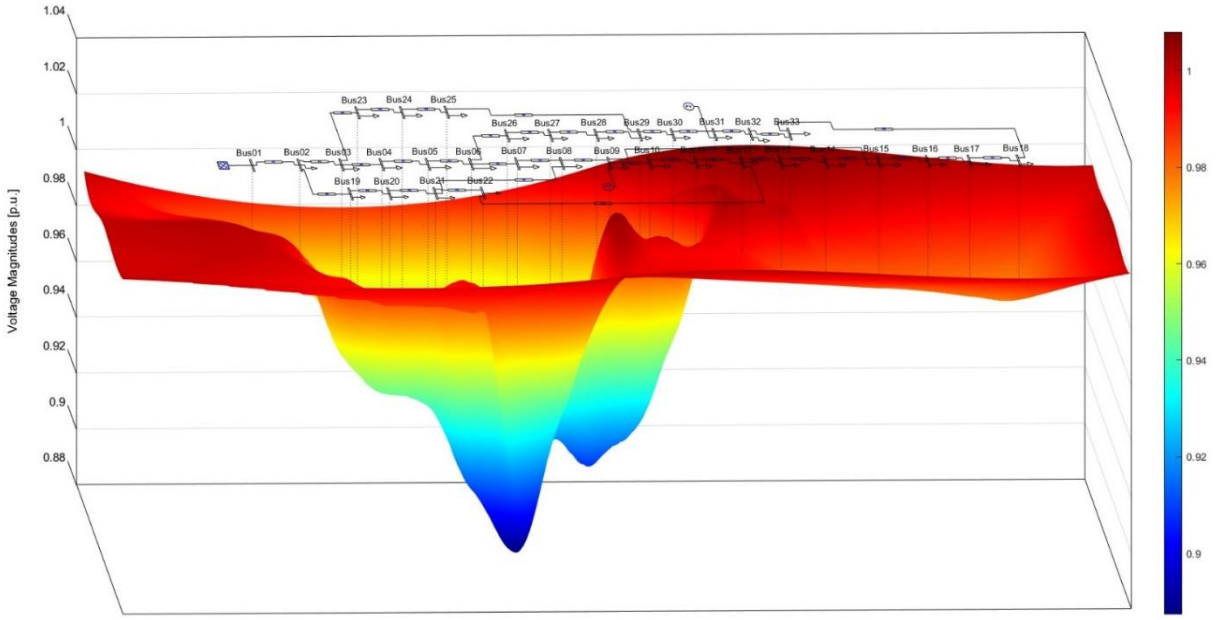

Fig.6 The bus voltage magnitudes of Case 5 using the GWO

Figure.6 shows bus voltage magnitudes for Case5 (GWO) in the IEEE 33-bus system. Higher voltages (0.98-1.0 p.u.) and reduced voltage drops (~0.88-0.92 p.u.) indicate improved stability and power distribution due to optimized tie- switching and PV placement that result revealed the voltage magnitude with minimize 0.983 p.u. and maximum 1.015 p.u. average 0.996 p.u..

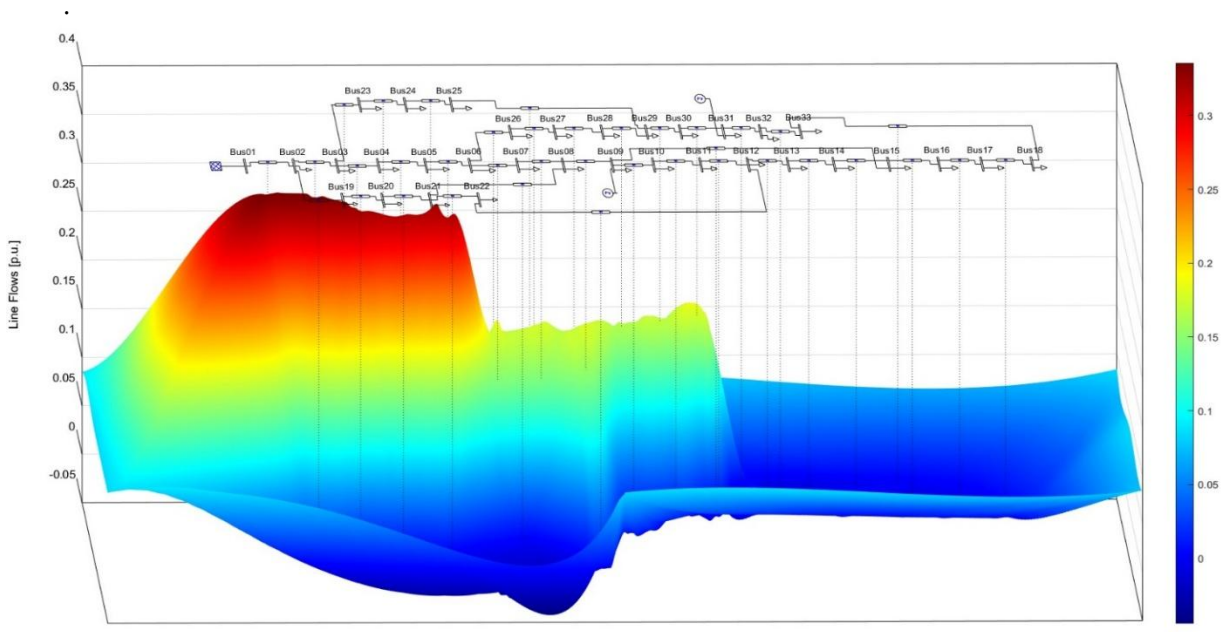

Fig. 7 The transmission lines power flow of Case 5 using the GWO

Figure. 7 shows optimized power flow in the IEEE 33-bus system with GWO. Balanced load distribution, reduced losses (blue regions), and minimized congestion (smaller red zones) confirm that tie-switching and PV placement enhance efficiency and stability.

Table 6 SIMULATION RESULTS OF PSO

Case	PVs		Tie Switch (No.)	Total power loss		Voltage Deviation		PF Control
	(kW)	(Bus No.)		Before (kW)	After (kW)	Before (p.u.)	After (p.u.)	
1	-	-	-	202.677	-	1.700	-	-
2	-	-	-	225.295	-	1.801	-	-
3	-	-	8, 6, 13, 35, 27	225.295	156.205	1.830	1.125	-
4	3000	28	10, 19,11,14,23	225.295	68.428	1.830	0.308	0.85
5	**1883, 1465**	**30,8**	**34, 18, 12, 14, 27**	**225.295**	**20.124**	**1.830**	**0.099**	**0.85, 0.85**
6	984, 2196, 223	9,29,18	32, 19, 12, 35, 21	225.295	19.059	1.830	0.123	0.85, 0.85,1
7	3,000	8	8, 19, 13, 30, 36	225.295	115.859	1.830	0.729	-
8	2367, 1335	8,31	34, 19, 12, 14, 35	225.295	107.332	1.830	0.468	-
9	1119, 779, 2099	3, 12, 30	32, 19, 33, 14, 23	225.295	101.076	1.830	0.627	-

Table. 6 highlights the effectiveness of PSO in optimizing PV placement and tie-switching. Baseline cases (1 & 2) exhibit high power losses (202.677 kW and 225.295 kW) with poor voltage deviation (1.700 p.u. and 1.830 p.u.). Tie-switching alone (Case 3) reduces power loss to 156.205 kW, (30.66% improvement), while adding PVs (Case 4) further lowers it to 68.428 kW. while adding PVs (Case 4) further lowers losses to 68.428 kW, improving voltage deviation to 0.308p.u. The most optimized scenario, Case 5, with 1,883 kW and 1,465 kW PVs at Buses 30, 8 and tie-switching at 34,18,12,14,27 achieves the lowest power loss (20.124 kW, 91.06% reduction) and the best voltage stability (0.099 p.u.) with optimal PF control (0.850, 0.850). Cases 6-9, despite larger PVs, do not surpass Case 5, underscoring the importance of strategic PV placement and switching. These results confirm PSO's effectiveness in enhancing distribution network performance.

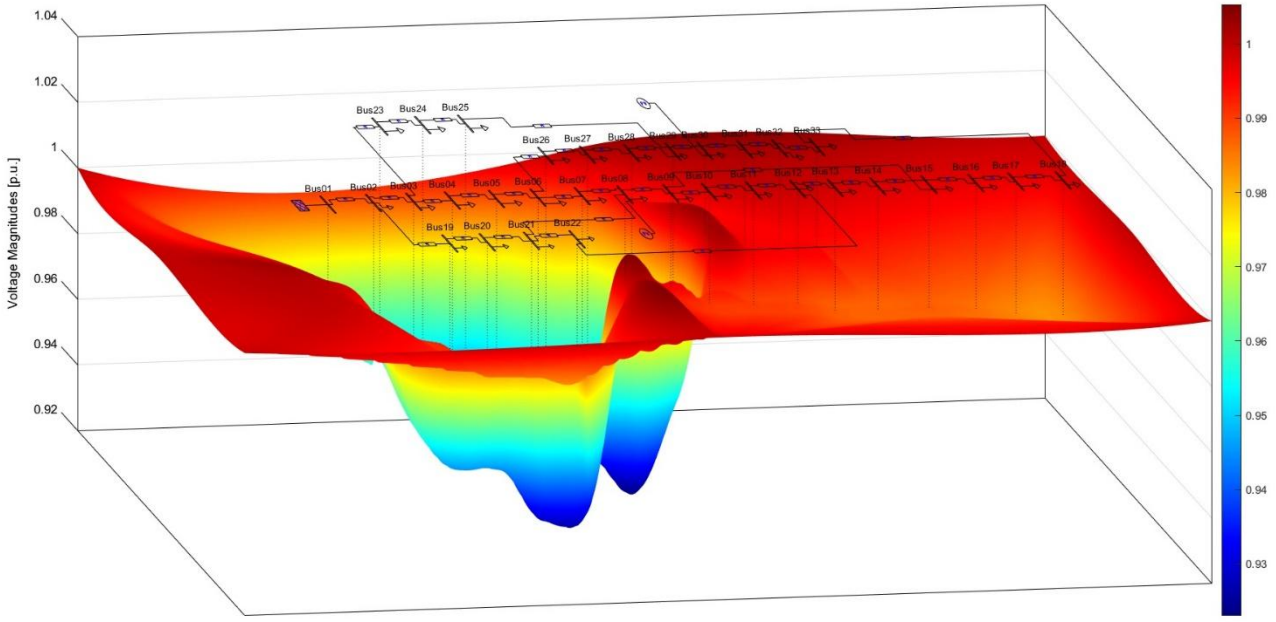

Fig. 8 The bus voltage magnitudes of Case 5 using the PSO

Figure. 8 shows bus voltage magnitudes for Case 5 (PSO) in the IEEE 33-bus system. Higher voltages (0.98-1.0 p.u.) and fewer voltage drops (0.93-0.95 p.u.) The voltage profile across the IEEE 33-bus system is shown with a color gradient, where red represents higher voltages

and blue indicates lower voltages which is minimum voltage: 0.992 p.u. maximum voltage: 1.005 p.u. average voltage: 0.997 p.u. confirm PSO's effectiveness in stabilizing voltage and optimizing power distribution.

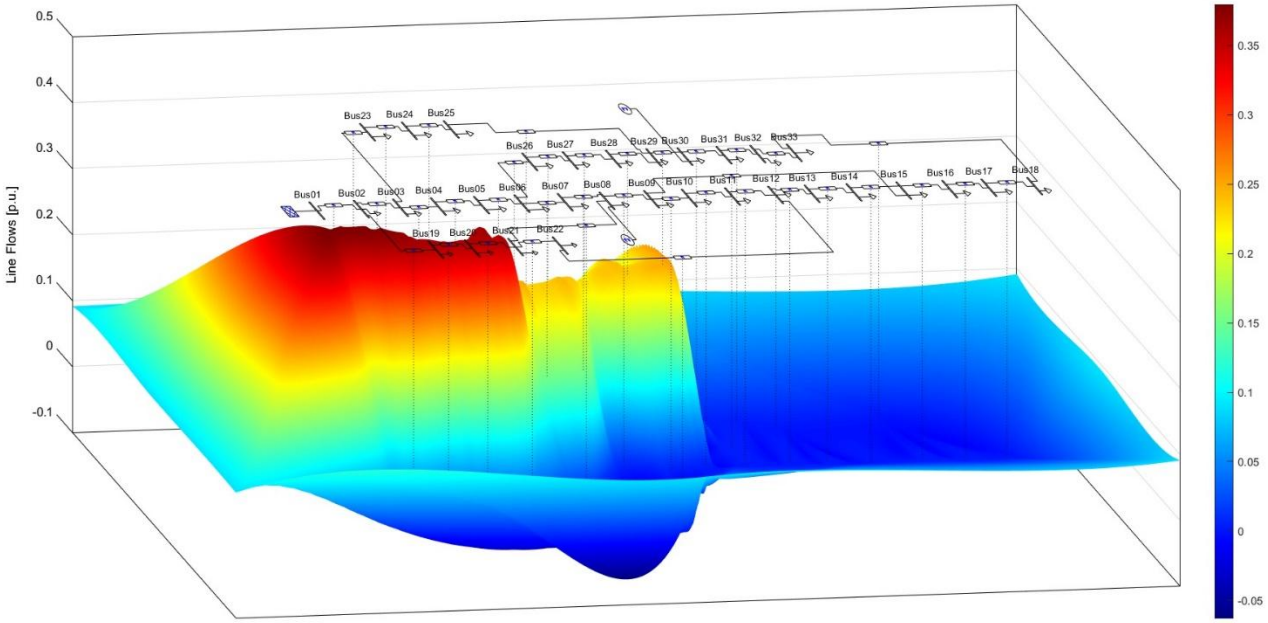

Fig. 9 The transmission lines power flow of Case 5 using the PSO

Figure. 9 shows optimized power flow in the IEEE 33-bus system with PSO. Balanced distribution, reduced losses (blue regions), and minimized congestion (smaller red zones) confirm PSO's effectiveness in improving efficiency and stability.

Table 7 Simulation Results of the WOA

Case	PVs		Tie Switch (No.)	Total power loss		Voltage Deviation		PF Control
				Before	After	Before	After	
	(kW)	(Bus No.)		(kW)	(kW)	(p.u.)	(p.u.)	
1	-	-	-	202.677	-	1.700	-	-
2	-	-	-	225.295	-	1.801	-	-
3	-	-	8,6,13,35,27	225.295	160.311	1.830	1.129	-
4	2,745	15	20,19,12,29,27	225.295	153.339	1.830	0.355	1
5	**2119, 1525**	**30, 8**	**20, 18, 13,15,22**	**225.295**	**28.191**	**1.830**	**0.135**	**0.913, 0.850**
6	1205, 1245, 432	18,6,13	9, 4, 12,28,23	225.295	199.601	1.830	0.199	0.850,0.850,0.850
7	1748	17	10,5,11,28,27	225.295	165.926	1.830	1.213	-
8	1388 ,1468	15, 25	20,6,11,29,27	225.295	70.566	1.830	0.708	-
9	1281, 1089, 781	29, 15, 30	20,6,12,35,22	225.295	90.159	1.830	0.585	-

Table 7. highlights the effectiveness of WOA in optimizing PV placement and tie-switching. Baseline cases (1 & 2) exhibit high power losses (202.677 kW and 225.295 kW) with poor voltage deviation (1.700 p.u. and 1.830 p.u.). Tie-switching alone (Case 3) reduces power loss to 160.311 kW, (28.84% improvement) while adding PVs (Case 4) further lowers it to 153.339 kW. while adding PVs (Case 4) further lowers losses to 153.339 kW, improving voltage deviation to 0.355 p.u. The most

optimized scenario, Case 5, with 2,119 kW and 1,525 kW PVs at Buses 30, 8 and tie-switching at 20, 18, 13,15,22 achieves the lowest power loss (28.191 kW, 87.48% reduction) and the best voltage stability (0.135 p.u.) with optimal PF control (0.913, 0.850). Cases 6-9, despite larger PVs, do not surpass Case 5, underscoring the importance of strategic PV placement and switching. These results confirm WOA's effectiveness in enhancing distribution network performance.

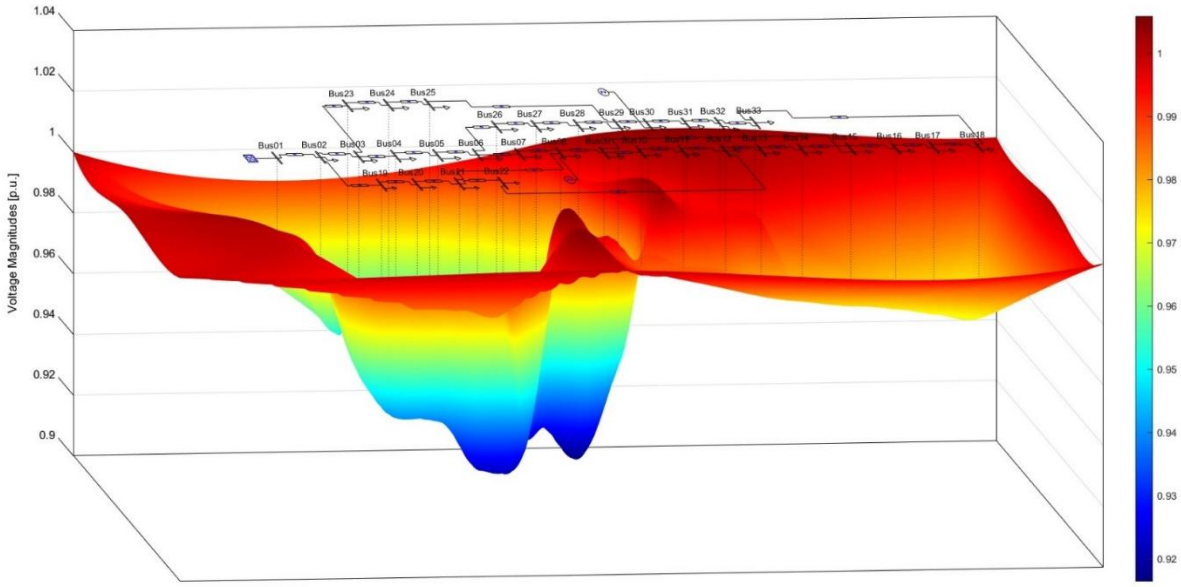

Fig. 10 The bus voltage magnitudes of Case 5 using the WOA

Figure. 10 shows bus voltage magnitudes for Case 5 (WOA) in the IEEE 33-bus system. Higher voltages (0.98-1.0 p.u.) and reduced voltage drops (0.92-0.94 p.u.) confirm WOA's effectiveness in stabilizing voltage and optimizing power distribution. The voltage profile across the IEEE 33-bus system is shown with a color gradient, where red represents higher voltages and blue indicates lower voltages which is minimum voltage: 0.986 p.u. maximum voltage: 1.003 p.u. average voltage: 0.996 p.u..

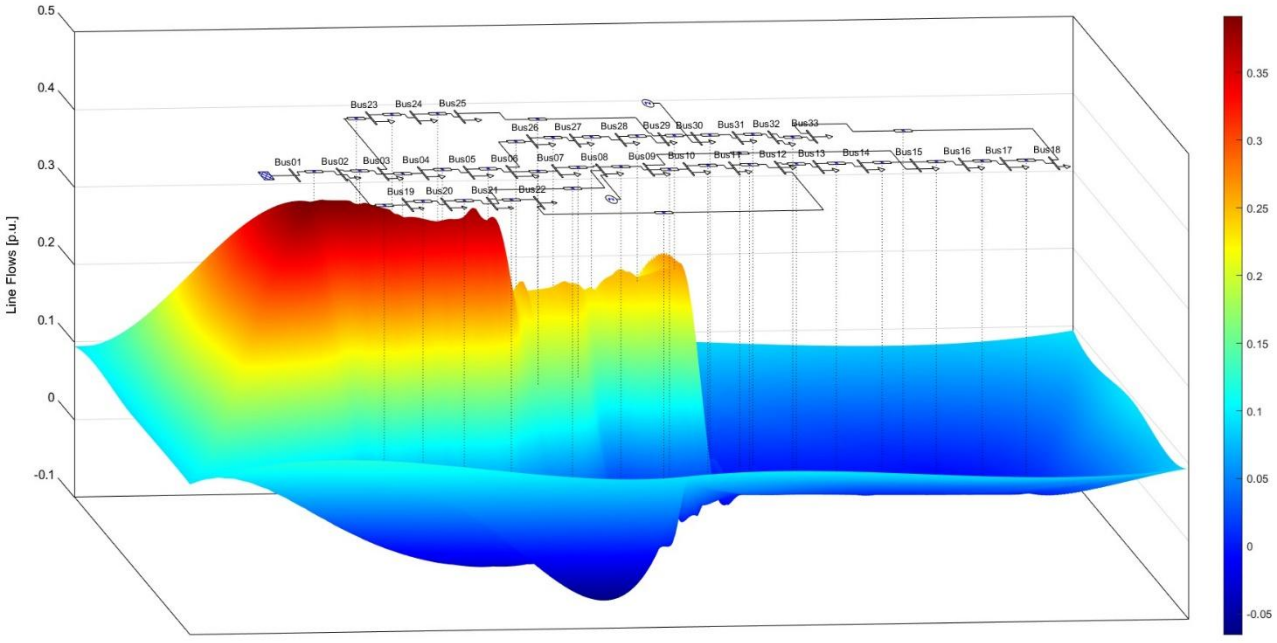

Fig. 11 The transmission lines power flow of Case 5 using the WOA

Figure. 11 shows optimized power flow in the IEEE 33-bus system with WOA. Balanced distribution, reduced losses (blue regions), and minimized congestion (smaller red zones) confirm WOA's effectiveness in improving efficiency and stability.

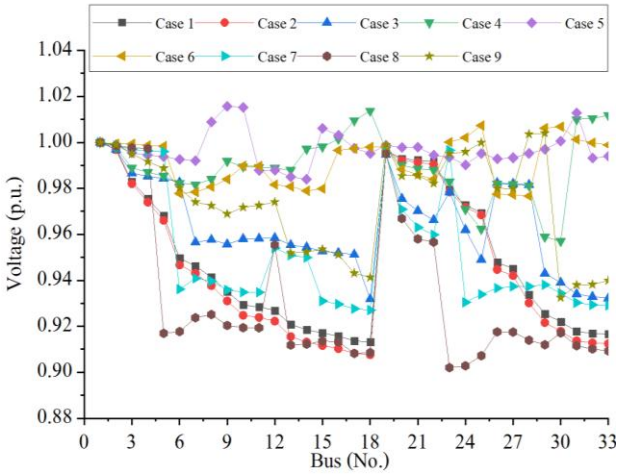

Fig. 12 An example of a graph GWO The difference of voltage magnitude

Figure. 12 compares voltage magnitudes across buses for different optimization cases using GWO. Baseline cases (Case 1 & 2) show the lowest voltage profiles, indicating significant drops. Case 3 & 4 (tie-switching and PVs) improve voltage stability, while Case 5 achieves the highest voltage support, ensuring the most stable profile. Other cases (6-9) show varying improvements but remain suboptimal. The results confirm that Case 5 optimally enhances voltage stability, demonstrating the effectiveness of GWO in PV placement and network reconfiguration.

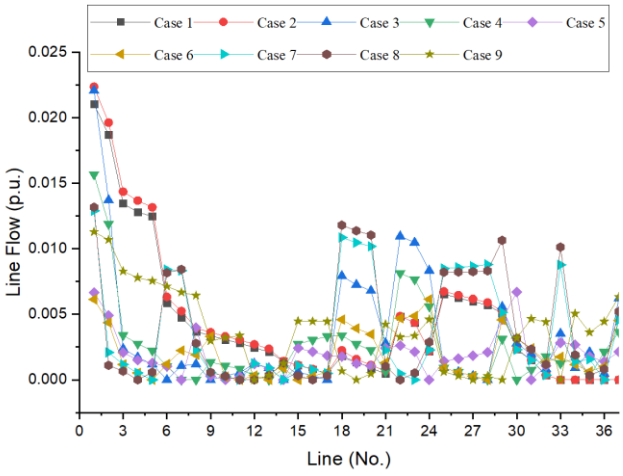

Fig. 13 An example of a graph GWO The difference of Line Flow magnitude

Figure. 13 compares line flow magnitudes for different GWO optimization cases. Baseline cases (1 & 2) show the highest line flows, indicating network congestion. Case 3 & 4 (tie-switching and PV placement) reduce flows, improving distribution. Case 5 achieves the lowest line flow, minimizing power losses and congestion. Other cases (6-9) show improvements but remain suboptimal. The results confirm that Case 5 optimally enhances network efficiency and stability.

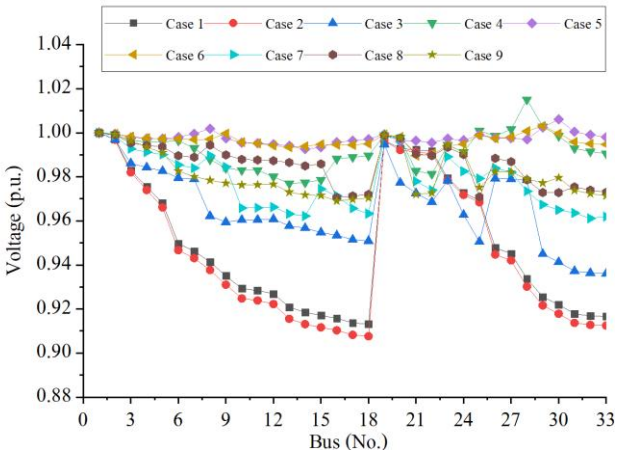

Fig. 14 An example of a graph PSO The difference of voltage magnitude

Figure. 14 compares voltage magnitudes across buses for different PSO optimization cases. Baseline cases (1 & 2) show the lowest voltages, indicating poor stability. Case 3 & 4 (tie-switching and PV integration) improve voltage regulation. Case 5 achieves the highest voltage stability, outperforming all cases. Cases 6-9 show moderate improvements but remain suboptimal. The results confirm that Case 5 provides the best voltage support, proving PSO's effectiveness in PV placement and network optimization.

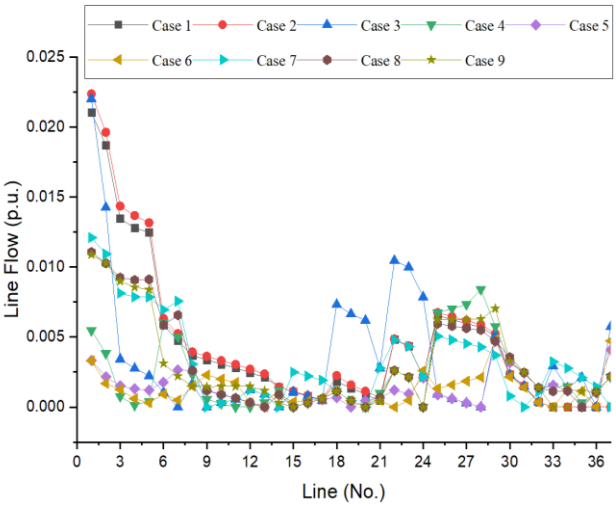

Fig. 15 An example of a graph PSO The difference of Line Flow magnitude

Figure. 15 compares line flow magnitudes for different PSO optimization cases. Baseline cases (1 & 2) show the highest congestion, while Case 3 & 4 (tie-switching and PV integration) reduce flows. Case 5 achieves the lowest line flow, minimizing losses and

improving power balance. Other cases (6-9) show moderate improvements but remain suboptimal. The results confirm that Case 5 optimally enhances network efficiency.

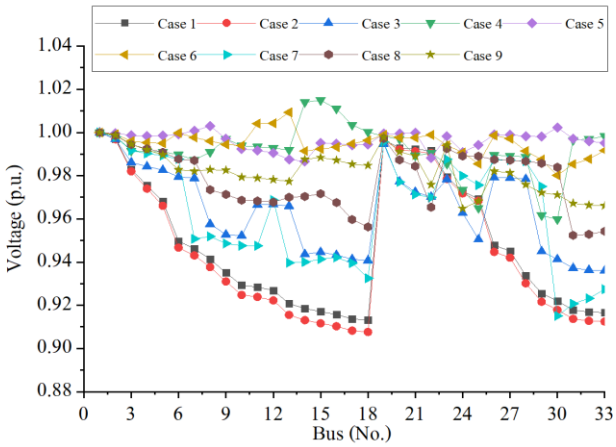

Fig. 16 An example of a graph WOA The difference of voltage magnitude

Figure. 16 illustrates voltage magnitudes across buses for different WOA optimization cases. Baseline cases (1 & 2) show the lowest voltages, indicating poor stability. Case 3 & 4 (tie-switching and PV integration) improve voltage levels. Case 5 achieves the highest voltage stability, ensuring the best overall performance. Cases 6-9 show moderate improvements but remain less effective. The results confirm that Case 5 optimally enhances voltage regulation, demonstrating WOA's effectiveness in PV placement and network reconfiguration.

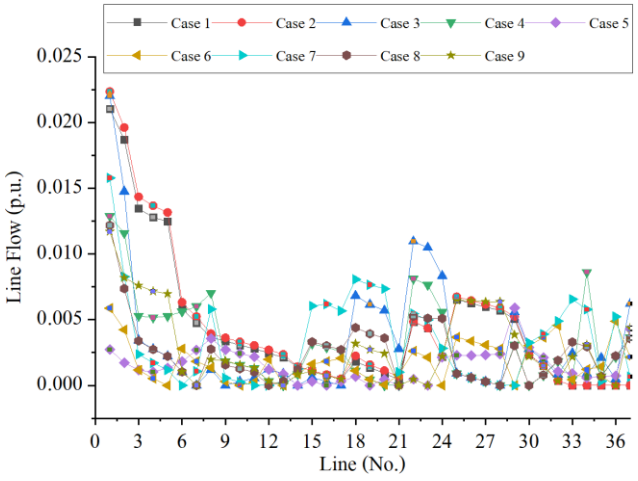

Fig. 17 An example of a graph WOA The difference of Line Flow magnitude

Figure 17 compares line flow magnitudes for different WOA optimization cases. Baseline cases (1 & 2) show the highest line flows, indicating congestion and losses. Case 3 & 4 (tie-switching and PV integration) reduce flows, improving power distribution. Case 5 achieves the lowest line flow, confirming optimal loss minimization and power balance. Cases 6-9 show moderate reductions but remain less effective. The results confirm that Case 5 optimally enhances network efficiency, demonstrating WOA's effectiveness in loss reduction and system stability.

Environmental performance indices are revealed by CO_2 emission reduction estimate the reduction in emissions due to optimal PV integration together with network reconfiguration and PV penetration level in Table 8. The emission factor is defined by 0.5251 kg CO_2/MWh.

Table 8 Comparison of the CO_2 emission reduction and the percentage of renewable energy level

Optimization Techniques	Best solution	PV power generation (kW)	CO_2 emission reduction (kg CO_2/MWh)	% Renewable (+FCS)
GWO	Case 5	2,756	2,376.99	68.64
PSO	Case 5	3,348	2,887.57	83.38
WOA	Case 5	3,644	3,142.87	90.76

Table 8 shows the Environmental performance indices with PV power generation and percentage of the renewable energy are presented the PV power generation can be reduced the CO_2 emission reduction. The results of CO_2 emission reduction and the percentage of renewable energy level are presented by PSO case 5 from the Table 6 in condition the lowest of minimize power loss can reduced the CO_2 emission of 2,887.57 kg CO_2/MWh with 83.38 % of the renewable utilization.

The simulation results highlight the significant impact of hybrid objective function for optimization techniques on enhancing power distribution network performance, improving voltage stability, and reducing environmental impacts. These findings demonstrate the practical applicability of the proposed methods in optimizing power loss, voltage regulation, and renewable energy integration. The knowledge gained from this research not only underscores the effectiveness of the hybrid optimization approach but also provides valuable insights into its potential guideline for real-world implementation. In the following section, we will discuss the broader implications of these results and offer recommendations for future research, along with practical applications across various distribution power system contexts.

5. Conclusion

This study analyzed the impact of FCS integration in the IEEE 33-bus radial distribution system, considering network reconfiguration, DERs, and control strategies. The results confirm that FCS integration increases power losses and voltage instability, but optimal tie-switching and PV placement significantly mitigate these effects. Among the optimization techniques PSO achieved the highest power loss reduction (20.124 kW, 91.06%), and optimal voltage stability. WOA provided a balanced performance, reducing losses by (28.191 kW ,87.48%). GWO effectively reduced losses by (50.776 kW, 77.45%),

while improving voltage profiles. The best-performing Case 5 across all methods demonstrated that strategic DER placement and network reconfiguration significantly improve power distribution efficiency, voltage stability, and system reliability. Furthermore, environmental benefits were evident, with CO_2 emission reductions highest in WOA (90.76%), followed by PSO (83.38%) and GWO (68.64%), emphasizing the role of optimized renewable energy integration. Overall, this research underscores the effectiveness of hybrid objective function for optimization techniques in enhancing the performance of power distribution networks. By employing a hybrid objective function and conducting a comparative analysis of three optimization algorithms GWO, PSO, and WOA the study offers a comprehensive and multidimensional evaluation. The findings clearly validate that the coordinated implementation of control strategies, alongside the optimal placement and sizing of photovoltaic generation units, substantially improves the operational efficiency and stability of the distribution system.

Acknowledgements

This research project is supported by Rajamangala University of Technology Isan. Contract No. FET006/2568. The opinions expressed in the research report are those of the grant recipients and do not necessarily reflect the views of the funding organization.

References

[1] M. A. Samman, H. Mokhlis, N. N. Mansor, H. Mohamad, H. Suyono, and N. M. Sapari, "Fast Optimal Network Reconfiguration With Guided Initialization Based on a Simplified Network Approach," IEEE Access, vol. 8, pp. 11948-11963, 2020, doi: 10.1109/access.2020.2964848.

[2] A. O. Salau, Y. W. Gebru, and D. Bitew, "Optimal network reconfiguration for power loss minimization and voltage profile enhancement in distribution systems," Heliyon, vol. 6, no. 6, p. e04233, Jun 2020, doi: 10.1016/j.heliyon.2020.e04233.

[3] U. Raut and S. Mishra, "An improved sine–cosine algorithm for simultaneous network reconfiguration and DG allocation in power distribution systems," Applied Soft Computing, vol. 92, 2020, doi: 10.1016/j.asoc.2020.106293.

[4] M. J. H. Moghaddam, A. Kalam, J. Shi, S. A. Nowdeh, F. H. Gandoman, and A. Ahmadi, "A New Model for Reconfiguration and Distributed Generation Allocation in Distribution Network Considering Power Quality Indices and Network Losses," IEEE Systems Journal, vol. 14, no. 3, pp. 3530-3538, 2020, doi: 10.1109/jsyst.2019.2963036.

[5] E. Kazemi-Robati and M. S. Sepasian, "Fast heuristic methods for harmonic minimization using distribution system reconfiguration," Electric Power Systems Research, vol. 181, 2020, doi: 10.1016/j.epsr.2019.106185.

[6] F. Hosseini, A. Safari, and M. Farrokhifar, "Cloud theory-based multi-objective feeder reconfiguration problem considering wind power uncertainty," Renewable Energy, vol. 161, pp. 1130-1139, 2020, doi: 10.1016/j.renene.2020.07.136.

[7] G. Srinivasan, "Optimization of distributed generation units in reactive power compensated reconfigured distribution network," Automatika, vol. 62, no. 2, pp. 249-263, 2021, doi: 10.1080/00051144.2021.1929741.

[8] L. Fu, W. Wang, Z. Y. Dong, and Y. Li, "Optimal Reconfiguration for Active Distribution Networks Incorporating a Phase Demand Balancing Model," IEEE Transactions on Power Systems, vol. 39, no. 5, pp. 6183-6195, 2024, doi: 10.1109/tpwrs.2024.3355127.

[9] L. Wang et al., "Enhancing Distribution System Restoration With Coordination of Repair Crew, Electric Vehicle, and Renewable Energy," IEEE Transactions on Smart Grid, vol. 15, no. 4, pp. 3694-3705, 2024, doi: 10.1109/tsg.2024.3353750.

[10] A. Pal, A. Bhattacharya, and A. K. Chakraborty, "Planning of EV Charging Station with Renewable based Generation in an Overlaid Network Considering Uncertainty and Traffic Flow," presented at the 2021 IEEE 4th International Conference on Computing, Power and Communication Technologies (GUCON), 2021. [Online]. Available: https://ieeexplore.ieee.org/document/9573944/.

[11] K. Yenchamchalit, Y. Kongjeen, P. Prabpal, and K. Bhumkittipich, "Optimal Placement of Distributed Photovoltaic Systems and Electric Vehicle Charging Stations Using Metaheuristic Optimization Techniques," Symmetry, vol. 13, no. 12, 2021, doi: 10.3390/sym13122378.

[12] M. Mazumder and S. Debbarma, "EV Charging Stations With a Provision of V2G and Voltage Support in a Distribution Network," IEEE Systems Journal, vol. 15, no. 1, pp. 662-671, 2021, doi: 10.1109/jsyst.2020.3002769.

[13] F. N. Lima, M. M. Santos, M. A. Benetti, T. Milke, and M. Sperandio, "Power Distribution Network Reconfiguration Considering the Transmission System Usage," IEEE Latin America Transactions, vol. 19, no. 12, pp. 2113-2121, 2021, doi: 10.1109/TLA.2021.9480154.

[14] W. S. Tounsi Fokui, M. J. Saulo, and L. Ngoo, "Optimal Placement of Electric Vehicle Charging Stations in a Distribution Network With Randomly Distributed Rooftop Photovoltaic Systems," IEEE Access, vol. 9, pp. 132397-132411, 2021, doi: 10.1109/access.2021.3112847.

[15] M. Z. Zeb et al., "Optimal Placement of Electric Vehicle Charging Stations in the Active Distribution Network," IEEE Access, vol. 8, pp. 68124-68134, 2020, doi: 10.1109/access.2020.2984127.

[16] X. Gan, H. Zhang, G. Hang, Z. Qin, and H. Jin, "Fast-Charging Station Deployment Considering Elastic Demand," IEEE Transactions on Transportation Electrification, vol. 6, no. 1, pp. 158-169, 2020, doi: 10.1109/tte.2020.2964141.

[17] N. Chitgreeyan et al., "Multi-Period Optimization of Energy Demand Control for Electric Vehicles in Unbalanced Electrical Power Systems Considering the Center Load Distance of Charging Station Areas," ENGINEERING ACCESS, vol. 10, no. 2, pp. 90-102, 2024, doi: 10.14456/mijet.2024.12.

[18] A. M. Shaheen, A. M. Elsayed, R. A. El-Sehiemy, and A. Y. Abdelaziz, "Equilibrium optimization algorithm for network reconfiguration and distributed generation allocation in power systems," Applied Soft Computing, vol. 98, 2021, doi: 10.1016/j.asoc.2020.106867.

[19] A. M. Shaheen, R. A. El-Sehiemy, S. Kamel, E. E. Elattar, and A. M. Elsayed, "Improving Distribution Networks' Consistency by Optimal Distribution System Reconfiguration and Distributed Generations," IEEE Access, vol. 9, pp. 67186-67200, 2021, doi: 10.1109/access.2021.3076670.

[20] N. Chitgreeyan, P. Pilalum, Y. Kongjeen, R. Kongnok, K. Buayai, and K. Kerdchuen, "Modified MATPOWER for Multi-Period Power Flow Analysis with PV Integration," GMSARN International Journal, vol. 19, no. 2, pp. 165-174, 2025.

[21] N. Chitgreeyan, Y. Kongjeen, K. Buayai, and K. Kerdchuen, "Impact of Voltage Unbalance System on Modern Microgrid System under High Penetration of Fast Charging Station," GMSARN International Journal, vol. 15, pp. 353-359, 2021.

[22] Olii, D., Kembuan, E. D., Rapar, J., & Takaredase, A. (2023). Analysis of the Voltage Stability of Power Using L-Index Voltage Stability. Technium, 17, 407–412. https://doi.org/10.47577/technium.v17i.10116

[23] https://ghgreduction.tgo.or.th/th/download-tver/120-tver-gwp-emission-factor/3377-emission-factor-30-2565.html

[24] Y. Li, X. Lin, and J. Liu, "An Improved Gray Wolf Optimization Algorithm to Solve Engineering Problems," Sustainability, vol. 13, no. 6, p. 3208, 2021. [Online]. Available: https://www.mdpi.com/2071-1050/13/6/3208.

[25] T. M. Shami, A. A. El-Saleh, M. Alswaitti, Q. Al-Tashi, M. A. Summakieh, and S. Mirjalili, "Particle Swarm Optimization: A

Comprehensive Survey," IEEE Access, vol. 10, pp. 10031-10061, 2022, doi: 10.1109/ACCESS.2022.3142859.
[26] Z. Wang, Y. Li, L. Wu, and Q. Guo, "A Nonlinear Adaptive Weight-Based Mutated Whale Optimization Algorithm and Its Application for Solving Engineering Problems," IEEE Access, vol. 12, pp. 40225-40254, 2024, doi: 10.1109/ACCESS.2024.3350336.
[27] L. Thurner, A. Scheidler, F. Schäfer et al, pandapower - an Open Source Python Tool for Convenient Modeling, Analysis and Optimization of Electric Power Systems, in IEEE Transactions on Power Systems, vol. 33, no. 6, pp. 6510-6521, Nov. 2018.
[28] N. Gholizadeh, "33-, 119-, and 136-bus system data for reinforcement learning-based distribution network reconfiguration," IEEE Dataport, August 28, 2023, doi: https://dx.doi.org/10.21227/m49t-q808.
[29] Abdullahi, Y. U. ., Oke, S., Rajan, J. ., Jose, S. ., & Oyediran Adedeji, W. (2024). Coupled Taguchi-Pareto-Box Behnken Design-Grey Wolf Optimization Methods for Optimization Decisions when Boring IS 2062 E250 Steel Plates on CNC Machine: doi: 10.14456/mijet.2024.4. Engineering Access, 10(1), 28–41. retrieved from https://ph02.tci-thaijo.org/index.php/mijet/article/view/247410